CISTER
Research Centre in
Real-Time & Embedded
Computing Systems

Journal Paper

Active Flow Control using Dense Wireless Sensor and Actuator Networks

Ramiro Robles*
Júlio C. Viana
João Loureiro*
João Cintra
André Rocha
Eduardo Tovar*

*CISTER Research Centre

CISTER-TR-180507

2018

Active Flow Control using Dense Wireless Sensor and Actuator Networks

Ramiro Robles*, Júlio C. Viana, João Loureiro*, João Cintra, André Rocha, Eduardo Tovar*

*CISTER Research Centre

Polytechnic Institute of Porto (ISEP-IPP)

Rua Dr. António Bernardino de Almeida, 431

4200-072 Porto

Portugal

Tel.: +351.22.8340509, Fax: +351.22.8321159

E-mail: rasro@isep.ipp.pt, joflo@isep.ipp.pt, null, null, emt@isep.ipp.pt

http://www.cister.isep.ipp.pt

Abstract

This paper describes the developments for the design of an active flow control (AFC) system for aeronautics applications based on dense wireless sensor and actuator networks (WSANs). The objective of this AFC system is to track gradients of pressure across the surface of the fuselage of commercial aircraft. This collected information is used to activate a set of actuators that will attempt to reduce the skin drag effect produced by the separation between laminar and turbulent flows. This will be translated into increased lift-off forces, higher vehicle speeds, longer range and reduced fuel consumption. The paper describes the architecture of the system in the context of the European research project DEWI (dependable embedded wireless infrastructure) using the concept of the DEWI Bubble and its three-tier architecture especially designed to ensure dependability and interoperability. A system-level simulator is also proposed to model each process of the AFC system and the DEWI Bubble infrastructure, highlighting the interactions between the network simulation and the results of the computational fluid dynamics (CFD) simulation. The key element in the solution is a patch of wired sensors and actuators, each patch provided with a wireless link to a central coordinator or access point conveniently located in the aircraft to maximize coverage to a network of distributed patches. A trade-off between capacity, scalability, size of the patch, fluid speed/viscosity, sampling sensor and actuator rates in space and time, and the capacity/delay characteristic of the wireless inter-patch and the wireline intra-patch communication technologies is also here discussed. The hybrid concept of wireless/wired network deployment achieves great flexibility, scalability, manageability, troubleshooting, and modularity as compared to a solution exclusively based on wireline or wireless components. The final details of the prototype and results in a wind tunnel test-bed are here described, demonstrating the validity of the concept and the use of wireless technologies for aeronautical applications. Future issues regarding security, safety and trustiness of the AFC system are also briefly introduced in the context of the spin-off European project SCOTT (secure connected trusted things).

Microprocessors and Microsystems 61 (2018) 279–295

Contents lists available at ScienceDirect

Microprocessors and Microsystems

journal homepage: www.elsevier.com/locate/micpro

Active flow control using dense wireless sensor and actuator networks

Ramiro Sámano*,[a], Julio Viana[b], Nelson Ferreira[b], João Loureiro[a], João Cintra[c], André Rocha[c], Eduardo Tovar[a]

[a] Research Centre in Real-time and Embedded Computing Systems, Porto, Portugal
[b] Critical Materials Lda., Braga, Portugal
[c] GMVIS SKYSOFT SA, Lisbon, Portugal

A B S T R A C T

This paper describes the design of an active flow control (AFC) system for aeronautics applications based on dense wireless sensor and actuator networks (WSANs). The objective of this AFC system is to track gradients of pressure (or wall shear stress) across the surface of the fuselage of commercial aircraft. This collected information is used to activate a set of actuators that will attempt to reduce the skin drag effect produced by the separation between laminar and turbulent flows. This is expected to be translated into increased lift-off forces, higher vehicle speeds, longer ranges and reduced fuel consumption. The paper describes the architecture of the system in the context of the European research project DEWI (dependable embedded wireless infrastructure) using the concept of the DEWI Bubble and its three-tier architecture especially designed to ensure dependability and interoperability in industrial WSANs. A system-level simulator is also proposed to model each process of the AFC system and the aeronautics DEWI Bubble infrastructure, highlighting the interactions between the network simulation and the results of the computational fluid dynamics (CFD) simulation. The key element in the proposed solution is a polygonal *patch* of wired sensors and actuators. This patch is provided with a wireless link to a central coordinator or access point conveniently located in the aircraft to maximize coverage to a network of distributed patches. A trade-off between scalability, size of the patches, fluid speed/viscosity, sampling sensor and actuator rates in space and time, and the capacity/delay characteristic of the wireless inter-patch and the wireline intra-patch communication technologies is also here discussed. The hybrid wireless/wired sensor and actuator network achieves great flexibility, scalability, manageability, troubleshooting, and modularity as compared to a solution exclusively based on wireline or wireless components. The final details of the prototype and results in a wind tunnel test-bed are here described, demonstrating the validity of the concept and the use of wireless technologies for aeronautical applications (flexible architecture and innovative services). Future issues regarding security, safety and trustiness of the AFC system are also briefly introduced in the context of the spin-off European project SCOTT (secure connected trusted things).

1. Introduction

Aircraft design in the aeronautics industry has been constantly evolving. Improved materials and more complex and sophisticated systems have boosted reliability and reduced safety risks. However, several issues remain to be addressed today. For example, the environmental impact of the ever-increasing number of flights needs to be reduced to comply with new regulations and tougher emissions control. This can be achieved through research and development of alternate fuel sources, novel engine technologies and structures, advanced concepts of aircraft surface morphing, improved aerodynamics, and air traffic management (ATM).

The reduction of fuel consumption is important for environmental protection purposes as well as for cost reduction. In the context of the European Union, the Cleansky framework addresses some of the main proposals to achieve up to 20% fuel consumption reduction in the aeronautical industry [1]. The potential to achieve this considerable reduction within the next 15 years can be attained by using a combination of aerodynamic, engine, and structural improvements [2–5], as expressed by the well-known Breguet range equation [6]:

* Corresponding author.
E-mail addresses: rasro@isep.ipp.pt (R. Sámano), jviana@critical-materials.com (J. Viana), njferreira@critical-materials.com (N. Ferreira), joflo@isep.ipp.pt (J. Loureiro), joao.cintra@gmv.com (J. Cintra), andre.rocha@gmv.com (A. Rocha), emt@isep.ipp.pt (E. Tovar).

https://doi.org/10.1016/j.micpro.2018.05.012
Received 26 January 2018; Received in revised form 18 April 2018; Accepted 15 May 2018
Available online 05 June 2018
0141-9331/

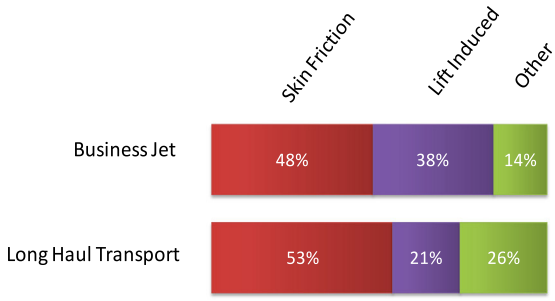

Fig. 1. Drag breakdown in commercial aircraft [3,4].

$$Range = \frac{velocity}{fuel\ \ consumption} \times \frac{lift}{drag} \times \ln\left(\frac{1 + W_{fuel}}{W_{payload} + W_{empty}}\right), \quad (1)$$

where W_{fuel} is the weight of the aircraft with fuel, W_{empty} is the weight of an empty aircraft, $W_{payload}$ is the weight of aircraft with payload, and $\ln(\cdot)$ is the natural logarithm. By inspecting the expression in (1) it is evident that technologies that reduce aircraft drag and the weight of an empty aircraft are crucial regardless of the selected aircraft configuration. *Aerodynamic drag* is known to be one of the factors contributing more to increased aircraft fuel consumption. In [3], a study shows that for a long-haul commercial aircraft (325 passengers) a combined reduction of 10% in both *skin friction* and *induced drag* (the components that roughly contribute around 80% to the total aerodynamic drag in such type of aircraft) may lead to a 15% fuel consumption reduction alone. The drag breakdown of a commercial aircraft shows that skin friction drag and lift-induced drag constitute the two main sources of drag, approximately one half and one third, respectively, of the total drag for a typical long range aircraft in cruise conditions [3,5] (see Fig. 1). Skin friction drag is therefore the main component of the aerodynamic drag. Skin friction arises from the friction of air against the "skin" of the aircraft. The primary source of skin friction drag during a flight is the *boundary layer separation*. The *boundary layer (BL)* is the layer of air moving smoothly in the immediate vicinity of the aircraft (wing, fuselage, tail) where the flow velocity is lower than that of the free air stream. Inside the BL, viscosity effects are relevant and thus viscous forces dominate. As the flow develops along the surface, the smooth laminar flow is disturbed developing a turbulent flow, which largely increases drag force (Fig. 2). In this transition, flow separation occurs due to a reversed flow at the surface, increasing drag (particularly pressure drag).

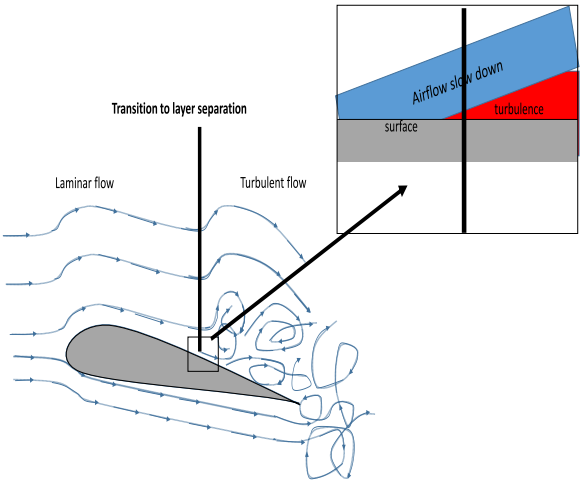

Fig. 2. Boundary layer (BL) transition exemplified with a wing profile.

Both BL transition and separation can be controlled in order to reduce drag. Skin friction can be reduced by keeping the flow in the laminar regime, thus reducing the extent of turbulent flow over the airfoil. Preventing flow separation will improve lifting and consequently reduce pressure drag.

The phenomenon of turbulence has attracted considerable attention over hundreds of years. Classic mechanics has successfully described fluids that behave in laminar regime. However, turbulent state description remains today as one of the main issues to be solved in the scientific world. Turbulence is the main regime that rules fluids in many aspects of nature. Laminar flows are therefore of very limited application. Turbulent flow modelling has countless numbers of applications in fields such as medicine, thermodynamics, motor design, biology, oceanography, cosmology, etc. A breakthrough in the understanding of turbulent flows over the surface of solid bodies was the concept of boundary layer introduced by Prandtl in [7]. The assumption is that the fluid speed at the boundary of the solid must be continuum, and therefore the flow speed must match (at the boundary) the speed of the solid layer. The concept of boundary layer provided us with a powerful tool to understand fluids in motion around solid objects and therefore in the formation or transition from laminar to turbulent regime in viscous fluids.

1.1. Approaches for aircraft skin drag reduction

The position of the BL transition is affected by local flow disturbances that can be caused by several factors, such as: surface roughness, vibration, heat, air-stream turbulence, or by manipulation of the pressure gradient produced by the flow on the surface. There are various approaches to reduce turbulent skin friction, involving different mechanisms, such as:

1. Reducing turbulent friction drag through riblets;
2. Deformable active skin using smart materials (compliant walls), or by
3. Locally delaying the boundary layer transition using vortex generators, such as, dimples, holes or *synthetic jet actuators* (SJAs).

In the case of SJAs, suction from the surface of the wing can be used to remove the low-energy air directly from the boundary layer. Additional momentum (high-energy air) can be achieved in SJA solutions by generating stream wise vortices near the edge of the boundary layer that re-energize the boundary layer flow.

A recent research work in [8] uses SJAs located at key positions on the wing to continuously energize the boundary layer and delay its separation. However, this approach does not use sensors to detect and trace the flow separation point, and is therefore static (passive) and proactive in nature. It results that the efficiency of static flow control is compromised and energy resources are wasted when there is no boundary layer separation or when it lies outside the actuators optimal control field. For this reason, active flow control (AFC) approaches have been proposed that allow for a convenient tracking of the BL via a network of sensors. Separation control was intensively studied in the past with mixed results. Novel sensor and actuator technologies point to a new generation of more efficient BL control technologies [10].

AFC is a multidisciplinary research field that integrates knowledge and exploits interactions of fluid mechanics, sensing, actuation and control systems, with the objective of improving aerodynamic performance. AFC has already been targeted by a number of research efforts (e.g., [2,5,9]). These works studied different aspects of AFC, including: the properties of AFC, the effects on energy consumption and proposed techniques to alleviate the wasted energy due to effects of skin friction drag. Other works have focused on the advantages of using continuous actuators [18], and the effects of using a feedback control on the turbulence to manipulate the turbulence sources [19]. The DEWI

prototype uses micropumps as a replacement of synthetic jet actuators. Recently, in [20], it has been shown that this type of active actuators has the potential to reduce almost to zero the skin drag effect when the flux created by the actuator or micro pump equals the speed of the flow parallel to the solid surface.

1.2. The DEWI bubble and the use of dense WSANs in AFC

DEWI (dependable embedded wireless infrastructure) is an ARTEMIS European project that focuses on the development of dependable wireless solutions for sensors and actuators in four industrial domains: *automotive, aeronautics, rail and building* [21]. DEWI is a project based on industrial use-cases that attempt to show the benefits of wireless sensor and actuator networks across different industrial domains. The core of the DEWI solution is the concept of the *DEWI Bubble*. A DEWI Bubble is a logical entity operating in a physical space delimited by the range of the wireless transmission technologies employed for intra-Bubble communications. A DEWI Bubble is a group of DEWI Bubble Nodes, DEWI Bubble Gateways and Users. They are located in short range to each other to ensure a local confinement. The Bubble may be organized in different topologies, whereas the organization may be distributed (ad-hoc network) or centralized with an access point. The DEWI bubble provides and encapsulation of different WSN technologies (legacy and new) with a single interface and format, thus contributing to the convergence and interoperability of different WSN and IoT standards.

The objective of the DEWI AFC is to employ the concept of the DEWI Bubble to enable the use of a hybrid wireless/wired architecture for the deployment of a dense network of sensors and actuators that will track and counteract the formation of turbulent flows across the surface of the fuselage of airplanes. The use of wireless technologies in industrial domains such as aeronautics has been always subject to issues of trust, reliability and security due to the inherent randomness of the media and the broadcast nature of the transmissions. This means that highly critical industrial applications were always built with cable infrastructure. The last few years, however, have witnessed a revolution of wireless standards and networks. The reliability of wireless standards has been improved and now they can complement or even replace some of their wireline counterparts.

In comparison with wireline solutions, wireless technologies provide flexibility in infrastructure deployment, coverage of places difficult to reach by cables, as well as over-the-air management and troubleshooting. In aeronautical and vehicular applications, the use of wireless is expected to bring lots of benefits (summarized in Table 1). Most of the weight of aircraft and vehicles are due to cabling infrastructure. The use of wireless as replacement of cables can bring benefits in reducing weight, which in turn can lead to savings in fuel consumption, increased payload and/or increase operational range. Reduce cabling infrastructure can also be translated in less man-hours for maintenance, troubleshooting, and in general less effort in infrastructure design. If wireless technologies cannot completely replace cables, due to criticality requirements, then they can be used as redundant links, thus combining the benefits of wireless and wireline solutions.

The DEWI Bubble aims to emphasize the main advantages of wireless solutions for industrial applications reinforcing dependability, interoperability and scalability. The DEWI Bubble uses a three-tier model for the encapsulation of heterogeneous wireless solutions (Level 0) interacting with internal real time wireline networks (Level 1) with a DEWI bubble Gateway that allows communication between Bubbles (Level 2) and external entities or the cloud. In this paper, wireless solutions are not used as replacement of cables. Instead, they are used to enalble a dense network of sensors scalable and modular, facilitating its deployment, management, troubleshooting, and cost effectiveness. The active flow control system uses patches of wired sensors and actuators, and each patch uses a wireless connection with an on-board access point. This means that the AFC systems uses a wireless network of patches, each patch being a wired network of sensors and actuators. The trade-off between the size of the patch, the communication requirements and the limitations of the wireless links to enable close-loop control and dissemination of actuation policies in the networks are discussed in this paper.

Table 1
Advantages vs. disadvantages of Wireless technologies in industrial applications [33].

Advantages	Disadvantages
Efficiency	**Electromagnetic susceptibility**
Weight reduction	***Quality of service degradation***
Decreased fuel consumption,	Increase of BER
Increased payload capacity,	***Decreased transmission rate***
Increased autonomy	Violation of deadlines
New/increased capabilities(indirect)	***Network collapse***
Dynamically reconfigurable	**Security issues**
Safety	***Confidentiality of data***
Self-redundancy	***Rejection of intrusions***
High survivability and resilience	***Survivability jamming signals***
Single-point-of-failure avoidance	**Power supply**
Self repairing capabilities	***Increased power consumption***
No wiring-ageing related problems	***Need for power supply***
Cost	Not always possible/desirable
Design and production	
No need of wire routing plans	
Flexibility gains design changes	
No wiring-related assembly tasks	
Maintenance, reparation & overhaul	
Ease of system maintenance	
Higher system integrity	
Reduced out-of-operation lines	
Increased scalability	
Withdrawal from service	
Simplified disassembly tasks	
Reduction of mass to be recycled	

The remainder of this paper is organized as follows. Section 2 describes the architecture of the DEWI AFC system. Section 3 describes the state of the art of sensors and actuators used in the AFC system. Section 4 presents the architecture of the system level simulator for the AFC system. Section 5 presents the details of the prototype and wind tunnel testbed. Section 6 presents the results of the computational fluid dynamics (CFD) simulation for a patch of actuators over a section of a wing profile. Section 7 present the final system-level and prototype measurement results. Section 8 presents a the scalability study of the system including compression, and finally Section 9 presents the conclusions of the paper.

2. System description and architecture

The objective of the DEWI Bubble AFC is to employ a wireless *sensor-actuator and communication bubble* for suppression of the turbulent flow and *delaying the BL transition*. The sensor network will detect the low-pressure region on the upper wing surface. The position of BL transition zone will be defined, selecting the appropriate actuators to be activated. At the same time, and based on the sensor values, the set of conditions for operation of the actuators (e.g., frequency, amplitude) will be calculated based on existing data (pre-set data). The selected actuators are activated to manage the turbulent flow on the wing surface. The data is stored. A new sensor reading is collected and the cycle is repeated. The stored data can be analysed to assess system operation during, for example, different flight profiles or moments (e.g., take-off, landing, and cruise) (see Fig. 3).

Ground systems can interact with the *sensor-actuator and communication bubble* to get the data recorded during the flight and process this information to determine appropriate actuation plans and analyse the data of the whole fleet. Fig. 4 depicts the approach to tackle the DEWI AFC system. There are several challenges in the interconnectivity

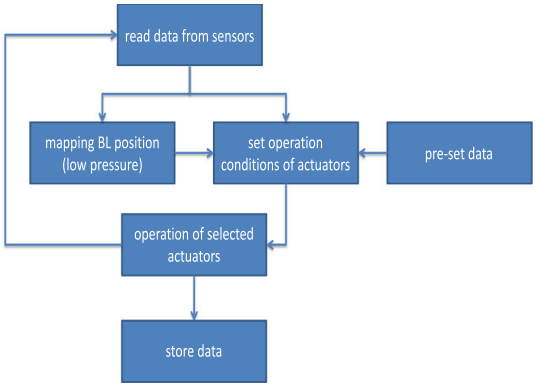

Fig. 3. Operation mode of the AFC system.

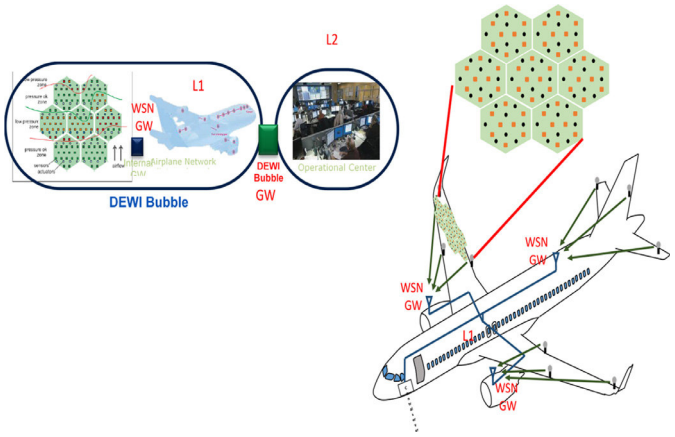

Fig. 4. Architecture of the DEWI AFC.

and how to achieve the desired objective in a dependable manner, whilst minimizing energy expenditure. The WSAN requires sensor measurements at high frequency and in a synchronous manner, to be able to correlate sensor readings, especially from sensors in close proximity. The WSAN also needs deal with failures of sensors, and this can be approached by employing reliable data transmission and data delivery mechanisms and also by employing data processing strategies that can deal with sensor failures.

It is important to boost the use of wireless communication systems on board to enable the deployment, as soon as possible, of technologies like structural health monitoring (SHM) and active flow control (AFC). To achieve this goal, these wireless networks and sensor systems need to communicate and interact with the main data buses of the aircraft. Hence, the specification of bi-directional bridges between different types of technologies is required. This is still the case if wireless technologies are used as the main data bus of the aircraft. Different wireless networks, with different delivery deadlines and different underlying technologies must operate together without possibility of interference. Bridge protocols and interfaces must be specified considering the constraints of the different networks.

The AFC system proposed by DEWI will comprise an architecture with a set of polygonal patches, each patch with a regular grid/array of sensors and actuators. These patches will be located mainly on surface of the wings of the aircraft, and potentially on other relevant surfaces of the fuselage. The objective is to control the turbulence region across the aircraft and reduce losses. All the sensors and actuators inside a single patch will be wired together sharing a single communication and control point. The patches will communicate wirelessly either with a relay or with an access point located conveniently in the aircraft to ensure good communication with several patches. Each patch will be enabled with some sort of intelligence to provide management of all the sensors and actuators inside the patch and to provide convenient communication link with the sink and the control unit inside the DEWI Bubble. The architecture of DEWI active flow control is therefore a hybrid of a wireless and wireline sensor network, which is the most convenient for this application. The information generated by each sensor will be collected by the control unit of each patch (DEWI node) which will provide some preliminary filtering, fusion and aggregation functionalities. The refined information will be then relayed towards the control unit (DEWI Gateway or relay node). Based on this collected information and based on different flight profiles, the AFC system will decide the type of actions to be performed by the set of actuators on each patch. Pre-set data for actuation policies are used as a look up table. Each patch can decide the best actuation policy according to the measured turbulence flow (closed loop). Each of the flow control actuators is a piezoelectric device (SJA or Fliperon). These actuators will allow the operator to change the boundary of the turbulence and thus help in counteracting the dragging effect in response to the measured information by the sensors and according to the current flight profile.

The size and number of patches, as well as the number of sensors/actuators per patch is optimized using a simulator. These parameters are function of the accuracy of the active flow control system, the range of the wireless technology selected, and the data rate of the wireless sensor nodes. All sensor/actuators nodes will be powered via cables. The patch will be provided with some power saving features too. For example, when a sensor information or actuation is not required from some patches, they can be powered down until they need to be used again, thereby saving energy.

The architecture proposed for the AFC system is relatively new in aeronautics, as it constitutes a hybrid design with wired and wireless components. The number of sensors for this application is expected to be large, more than in common WSNs, being deployed over a relatively small area. This brings up the issue of interference, provided each sensor was enabled with an individual wireless connection. To solve this problem, our approach presents an architecture where groups of sensors are wired together forming a patch that will act as a single wireless transmitter. Each patch will be provided with smart self-configuration and control. Fig. 5 shows the possible embodiment of a regular design of sensor and actuators inside a patch. Each patch will have a radio transceiver and a control unit with some intelligence. This DEWI node will be in charge of organizing the processing and operations inside the patch, as well as filtering, fusing, and aggregating data to be sent towards the wireless node (sink or DEWI Bubble Gateway).

Another important part of the AFC system is the interconnection of the wireless network into the avionics internal communication systems as shown in Fig. 6. The proposed solution has to be able to pass reliably the traffic from/to the wireless sensor/actuator network to the internal avionics network under different quality of service constraints. In general, the AFDX (avionics full-duplex switched ethernet) network (or ARINC664) has more stringent quality of service requirements, therefore the solution must include an appropriate scheduler that will ensure these quality of service constraints of the AFDX traffic are met or conveniently addressed when transported to/from the wireless domain.

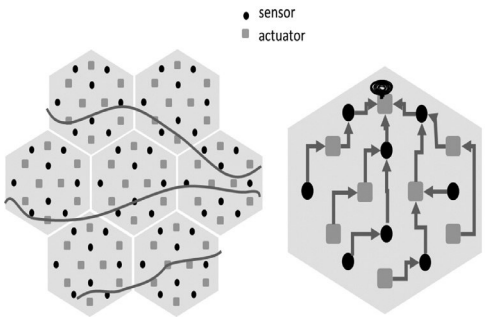

Fig. 5. Array of patches of sensors/actuators.

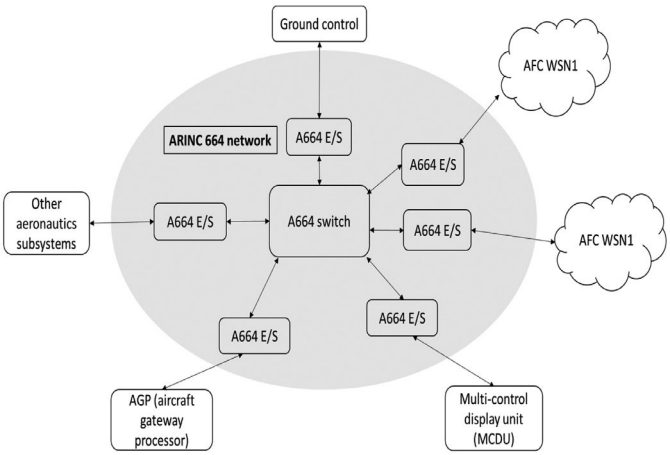

Fig. 6. DEWI AFC (Interaction with internal avionics networks).

3. Micro-sensors and actuators

3.1. Microsensors

Sensors for AFC applications need to be easy to install, non-invasive or with minimum flow disturbance, and able to detect and estimate the near-wall flow state, e.g., by means of measuring local pressure or shear stress. Techniques to measure wall shear stress can be categorized as: *thermal, mechanical* and *optical*. A particularly attractive solution is the micro hot-film shear stress sensor which has been conventionally associated with the field of MEMS (micro-electro-mechanical systems). There are basically three different ways to sense with this kind of sensors. A control circuit keeps either the temperature, current or voltage at a constant value, and by means of measuring the non-fixed parameter, it is possible to indirectly estimate the shear stress, e.g. by measuring the heat loss in the exposed hot-film. There are some issues related to this kind of sensors regarding heat loss to the substrate, problems in measuring the flow direction, and consequently in resolving vortices orientation. However, many advances have been made over the last few years, and good results have been achieved with this kind of sensors. For example, in [11] a MEMS sensors array with forty sensors was constructed over an area of 70 × 70 mm, with a sensor spacing of 1.5 mm.

Recently, two consecutive European projects called AEROMEMS and AEROMEMS II (Advanced aerodynamic flow control using MEMS) [12], addressed the integration and cost/benefit assessments of MEMS flow separation control technology used to improve the performance of wing high-lift systems, engine nacelles and turbo-machinery components. These projects addressed further development of prototype MEMS flow sensors and actuators of the previous EU funded projects. The objective was to improve efficiency and to address the issues of robustness associated with engineering integration. In this context and under the same operational principle, the authors in [13] presented a double hot-wire sensor, which was called hybrid AeroMEMS sensor array. It was a combination of a flexible printed circuit board (PCB) and a number of MEMS double hot-wires, single wires in different sensors setups, with each sensor featuring an area of 800 × 600 μm. As an improvement over the single hot-wire, the double sensor was able to measure the flow direction. Tests were conducted in a wind tunnel demonstrating its applicability in determining flow speed and directions, showing efficiency in determining the boundary layer separation. By means of numerical optimization it was shown that the thermal field pattern increases the frequency response. Under the same project in [13], but with another approach, the authors designed a high-resolution AeroMEMS sensor array for pressure measurements. The sensor cell is composed of a diaphragm with piezoresistor located at the edges of the cell. Measurements were based on the longitudinal and transversal piezo-resistive effect. A 2.5 × 4.5 × 0.3 mm chip was constructed, composed of a 900 × 900 μm diaphragm with a satisfactory sensitivity and frequency response of up to 160 kHz. An array of 13 sensors was mounted on a cylinder in a wind tunnel in order to compare the measurements with the theoretical expected values. The results led to the construction of a fully functional and reliable sensor. Schober et al. [14] have developed a MEMS surface fence sensor for skin friction measurements. The fence equipped with piezoresistors is 300 μm high and 5 mm long with a resolution of the wall shear stress of 0.02 Pa, and a temporal resolution up to 1 kHz. Another approach is the micropillar sensors for wall-shear-stress measurement, initially inspired by the hair cell or the lateral line of a fish. Preceded by Jonathan et al. [15], Chen et al. [16] reported that water flows as low as 1 mm/s can be measured with their MEMS pillar sensor using doped-silicon piezo-resistive strain gauges and an epoxy pillar.

3.2. Actuators

The field of AFC has experienced an explosive growth reflected on the variety of actuators. This is evidence of both the importance and challenges associated with actuators design. Actuators are basically transducers that convert an electrical signal to a desired physical quantity. The active flow actuators modify a flow by means of electronically controlled disturbances, which can be generated in many different ways. This section presents the state-of-the-art overview and an analysis of the possible application of the different types of actuator in the AFC system, mainly based on spatial and temporal requirements.

There are various types of actuators used in flow control applications with different operational principles. Cattafesta and Sheplak [17] suggested a classification in which the actuators are organized based on their functionality, as illustrated in Fig. 7. A common type of actuator is fluidic, which is based on the fluid injection and suction from/to the environment. Periodic excitation (injection/suction) is preferable rather than steady flow because the flow can be excited at natural (intrinsic) frequencies of the instabilities in the separating flow.

Two other kinds of actuators are derived from this main concept:

1. Zero-net mass-flux (ZNMF), also called *synthetic jet actuators* (SJAs). In these actuators the amount of air blown out and sucked in is the same; and
2. Nonzero mass-flux.

The first type of actuator is generally based on a diaphragm which ingests or/and expels fluid (air) through an orifice/slot in an oscillatory manner, using only the working fluid with no external mass source/sink. Nonzero mas-flux devices, on the other hand, can also ingest or

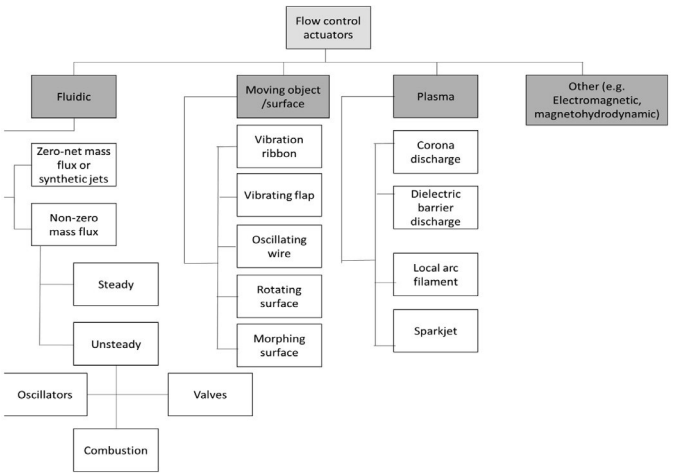

Fig. 7. Flow control actuators classified by function.

expel fluid from/to a source/sink. They can operate in a steady or unsteady state, like pulsed jets, natural fluidic oscillators, and combustion-driven devices. They can range in scale from conventional macro-scale to microjets.

Typical fluidic devices are based on piezoelectric or electrodynamics diaphragm. The diaphragm oscillates about its equilibrium position, alternately expelling/ingesting fluid from/into its cavity. SJAs have been applied in various flow control applications, including separation control and jet vectoring [18]. Diez and Dahm [22] have proposed a dense array of SJAs and obtained a flat frequency response up to 10 kHz with a relatively low driving voltage of 15–20 V.

Other type of actuator involves a moving body inside or on the boundary layer. Although fluidic devices usually involve some moving mechanical part, the main function is fluidic injection or suction. Alternatively, the purpose of the moving object is to induce modifications on the local flow motion. This can be performed by vibrating flaps, time-periodic motion of a surface mounted diaphragm, an oscillator wire, rotating surface elements and morphing surfaces. These can take various forms, among which the most common are the piezoelectric composite flaps and electro active dimples. Suzuki et al. [23] developed magnetic flap actuators with a copper coil on polyimide film for jet mixing control. They obtained a 0.4 mm tip displacement at a current of 1 A and a resonant frequency of 270 Hz. The two types of actuator discussed here are illustrated in Fig. 8. The last class here considered is solid-state actuators, also called plasma actuators, which have gained popularity because of the lack of mechanical parts and because of its short response time. The most popular one is the *single dielectric barrier discharge* (SDBD) plasma actuator, which consists of an asymmetric pair of electrodes separated by a dielectric material. An AC waveform with voltages between 1 and 30 kV and frequencies from 50 to 20 kHz is supplied to the exposed electrode. This results in an asymmetric electric field which ionises the air molecules, forming locally cold plasma. The accelerated charged particles transfer momentum to the surrounding gas, adjacent to the surface, via collisions with neutral particles, causing the desired flow disturbance. The work in [24] presents how to implement two different flow control techniques for skin friction that achieved a 45% reduction. Experimental results were obtained using different modifications to the near-wall structures depending on the control technique.

4. Simulator architecture

4.1. Fluid modelling domain

The architecture of a simulator must closely follow the architecture of the system to be simulated. The simulator architecture is shown in Fig. 9. The first block of the simulator is the computational fluid dynamics (CFD) block which is in charge of the simulation of the turbulence boundary layer separation and the effects of actuators. The CFD block provides the information for the network of sensors that will be able to track the boundary layer that separates the laminar from turbulent flows. This information will be therefore our traffic model input for the wireless sensor network and the patch configuration. It is not possible to conduct a simultaneous CFD and WSAN simulations due to complexity constraints. Therefore, the results of CFD must be computed off-line and then imported into the simulator via an interface model. Different interface and instability models have been implemented in the simulator to obtain the statistics of the separation processes across the surface of a wing. The boundary layer process is considered as a bi-dimensional space-time stochastic process that can be modelled as a random envelope with spatial and temporal correlation properties. These correlation statistics depend on the speed of the fluid, viscosity, and the angle of attack. The simulator also has the option of using its own instability model based on the concept of propagator matrix commonly used in instability analysis of flows. All interface models have been implemented for the whole duration of an aircraft missions considering different angles of attack. Therefore, the simulator can reproduce the flight conditions of different aircraft, which is an attractive aspect for applications of traffic and fleet management in the context of smart aeronautics applications.

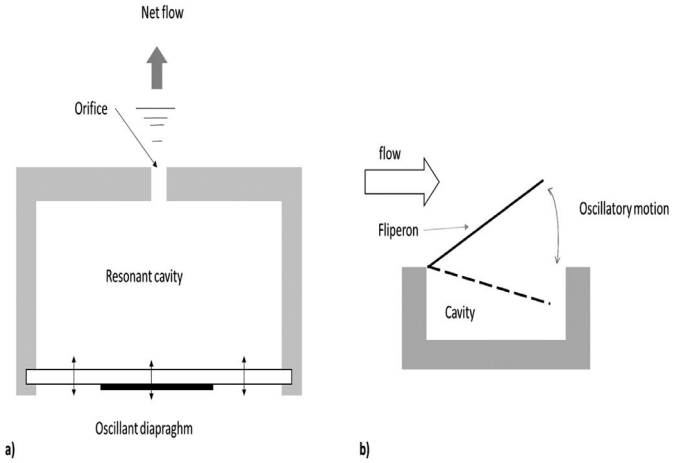

Fig. 8. Flow control actuators: a) SJA; b) Fliperon.

4.2. Sensor and actuators configuration: patches

The network of sensors and actuators is organized in patches. The number of sensors and actuators per patch, as well as their spacing and positions within the patch can be configured in the simulator. This also defines the size of the patch and the number of patches used to cover a designated area over the fuselage of the aircraft. The simulation tool includes options for the internal network of sensors and actuators. It enables the design of an internal network of processors communicating readings through the wired network. This configuration allows us to study the real-time properties of the intra-patch communication and evaluate delay, packet error performance, etc. An important aspect included in the intra-patch network design is the implementation of compression algorithms that allow for a reduction on the requirements of communication bandwidth to transport sensor readings inside and outside the patch. The simulation tool includes an option to implement compression algorithms, particularly those related to boundary detection. The main interest of the network of sensors is the detection of the boundary layer separation between laminar and turbulent flows. The idea of the network of patches is that different levels of the network can process different levels of statistics of the airflow. This means that faster statistic of turbulent flow can be only processed inside the patch and potentially at each sensor and actuator elements. Slower changes of turbulent flow can be relayed from each patch towards the internal aeronautics network, where the statistics of all the patches of the aircraft can be monitored and processed. Fine tuning of the actuation profile can be performed for the network of patches on board each aircraft. One more level of processing can be enabled at ground control, where the measurements of a complete fleet of aircraft can be processed and analysed.

4.3. Wing design, aircraft configuration, and propagation modelling

The simulator also allows for different aircraft configuration of different sizes and more importantly different wing profiles using the NACA (National Advisory Committee for Aeronautics) series. A user of the simulator can configure the coefficients of symmetrical and non-symmetrical NACA airfoil profiles. The configuration of the aircraft also defines the propagation electromagnetic model, which is crucial for the evaluation of the wireless component. Several propagation models have been included in the simulator (e.g. ITU WAICs -wireless avionics

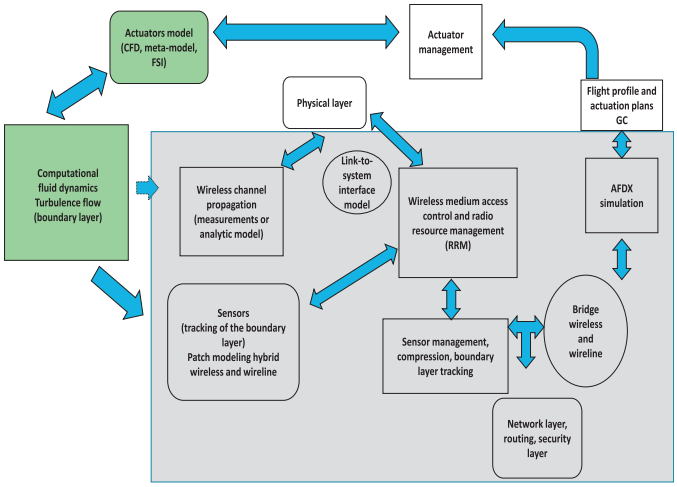

Fig. 9. Simulator architecture.

intracommunications- model [34]), including our own calculated metrics using ray tracing algorithm. The simulator can also include other propagation models and fit the best or mixture of the best models according to the scenario considered. The channel model is used for the evaluation of the physical (PHY) layer of the wireless technology in use, which is related to the modulation format, encoding, frame definition, power and signal processing operations. The PHY-layer must interact with the simulator mainly via a compression model. The joint simulation of PHY and upper layers is in general too complex to be included dynamically in the same software tool. PHY-layer simulations are usually conducted off-line and the results are imported into the main simulator via look-up-tables or link-to-system-level interface (LSLI) compression models.

4.4. Radio resource management and bubble gateway

The core of the simulator is the block in charge of allocation of resources, conflict resolution and in general of medium access control (MAC) functionalities. This block is in charge of obtaining the PHY-layer performance from the LSLI abstraction model, generate performance metrics at the radio resource or packet data level and obtain system level metrics such as throughput, fairness, outage probability, service area, coverage, and geographical information transfer rate (multi-hop settings). This block is also in charge of the self-configuration, multi-hop routing, management of sensor nodes, and also it has an additional functionality of the sensor data management, which in our case is the information of the boundary layer separation between the turbulent and the laminar flows.

An important part of the simulator is the bridge between the wireless network and the internal wireline aeronautical network of the aircraft. This bridge operation requires accurate modelling mainly because of the upper layers have different characteristics, requirements, delay deadlines, quality of service requirements that must be addressed by an appropriate proxy server and scheduling technology. The AFDX and the wireless sensor network can be simulated using different instances of the same simulator that communicate with each other via web-services or using a virtual distributed framework for interconnection of simulators, which have been previously proposed in other European projects.

The internal network of the aircraft relays the boundary layer sensed information to ground control which will be in charge of selecting proper actuating policies based on different flight profiles. The selected actuation profile is then communicated to the network of actuators to perform changes intended to reduce the turbulent flow formation.

4.5. Metrics and evaluation

A number of metrics will be implemented to evaluate the performance of the design. Two types of metrics will be used: one set for the fluid domain, and the other set of metrics for the wireless domain.

4.5.1. AFC metrics

1. Lift vs. angle of attack. The average lifting force experienced by the section of the wing under analysis
2. Skin drag reduction. The average reduction of drag due to turbulent flow formation
3. Boundary layer delay. The ability of modify the pattern of turbulent flow to a given specification.
4. Fluid velocity profile. The profile of velocity experienced by particles of the fluid.
5. Latency actuation. The time required for the system to react to sudden changes in the turbulence profile.
6. Fuel consumption reduction. The average reduction of fuel consumption with respect to non-actuation.

4.5.2. Wireless sensor network metrics

1. Coverage. The size of the geographical area where a given quality of service of wireless connection can be guaranteed.
2. Throughput. The average amount of information correctly transmitted per unit of time,
3. Goodput. the number of useful information bits delivered by the network to a certain destination per unit of time
4. Fairness. The measure of the equality between nodes in terms of statistical access to resources of the network.
5. Delay. The average period of time that information takes to be transmitted through the network.
6. Number of hops. The average number of hops that information takes to be transmitted through the network.
7. Backlog. The amount of information remaining to be retransmitted in the network
8. Block error rate. The average rate of errors per block of transmitted information
9. Distortion of sensing information. The measure of the error of the sensed information
10. Boundary layer tracking accuracy. The measure of the error in the correct tracking of the turbulent flow.

5. Prototype and testbed description

5.1. Wing section profile

The main objective in the design of a wing for any aircraft is that the profile achieves good levels of lift-off forces. In the laminar regime, a differential of pressure is created between the bottom and top sides of the wing, thus creating a force in the upward direction. Wing profiles are created using templates that have been previously designed to achieve different levels of lift-off forces under different values of angle of attack, wind speed, material weight, etc. Further details on the design of aircraft wings can be found in [23]. The most well-known profile templates for wing design are the NACA (national advisory committee for aeronautics) series. Each series is created by following a mathematical polynomial function with different numbers of parameters or coefficients. The formula for the shape of a NACA 00yy foil, with "yy" being replaced by the percentage of thickness to chord, is [30]:

$$y_t = 5t\left[0.2969\sqrt{\frac{x}{c}} - 0.1260\frac{x}{c} - 0.3516\left(\frac{x}{c}\right) + 0.2843\left(\frac{x}{c}\right)^3 - 0.1015\left(\frac{x}{c}\right)^4\right] \quad (2)$$

where: c is the chord length, x is the position along the chord from 0 to c, y_t is the half thickness at a given value of x (centerline to surface), and t is the maximum thickness as a fraction of the chord (so t gives the last two digits in the NACA 4-digit denomination divided by 10). The main parameters of the NACA airfoil profiles are shown in Fig. 10. For example, the NACA0024 airfoil profile (indicates that 4 digits were used for the calculation of the profile: 0, 0, 2, and 4. The NACA0024 profile has been selected for use in the DEWI AFC system. This profile is displayed in Fig. 11.

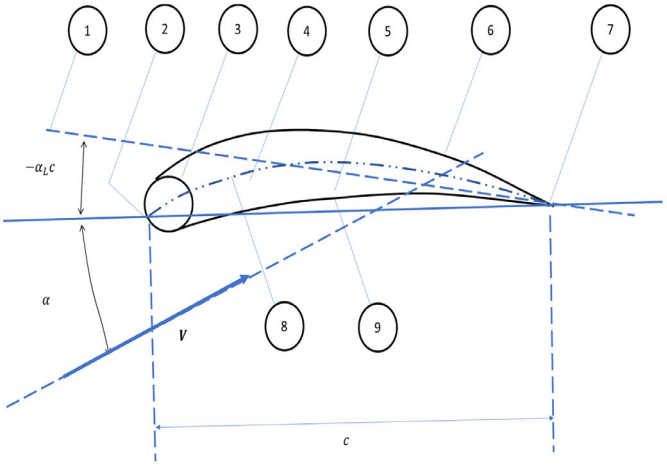

Fig. 10. 1: Zero lift line; 2: Leading edge; 3: Nose circle; 4: Max. thickness; 5: Camber; 6: Upper surface; 7: Trailing edge; 8: Camber mean-line; 9: Lower surface [23].

The final wing sections used in the AFC prototype using different types of material are displayed in Fig. 12. All wing profiles were constructed using the NACA0024 template. In some of our testing platforms, only half section of a wing was used due to the simplicity of wind tunnel design and pressure measurement.

5.2. Patch description

The central component of the architecture of the DEWI AFC system is the patch of sensors and actuators. Each patch contains a given numbers of sensors and actuators wired together and subject to a common control inside the patch. The patch is connected via wireless links to a sink or to the access point located conveniently in the aircraft (see Fig. 4). Patches are coordinated to be able to track the changes of pressure across the surface of the wing of an aircraft (see Fig. 1 for an illustration of boundary layer separation) and be able to actuate accordingly in an attempt to restore the laminar characteristics of the flow. This is intended to reduce the friction drag created by the separation of laminar and turbulent flows, and increase lift off forces. The size of the patch and therefore the number of sensors and actuators have been optimized according to the results of CFD simulation in Section 6.

The layout of the optimized patch of sensors and actuators is displayed in Fig. 13. The half wing section is used to position the sensors and actuators inside the patch as described in the previous layout is given in Fig. 14. The electronics used to control each micro-blower (actuator) and collect information from each sensor inside the patch are illustrated in Fig. 15.

A mock-up of the upper chamber of a NACA 0024 instrumented with the integrated active cell was built for preliminary tests (see Fig. 16). A full wing with actuators and sensors implemented over the surface is illustrated in Fig. 12.

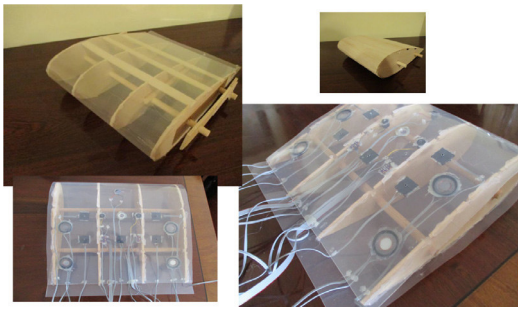

Fig. 12. Wing sections used for testing of the Active flow control system.

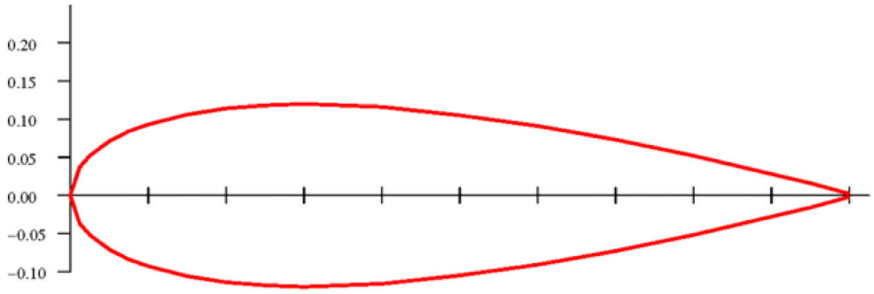

Fig. 11. NACA 0024 profile template.

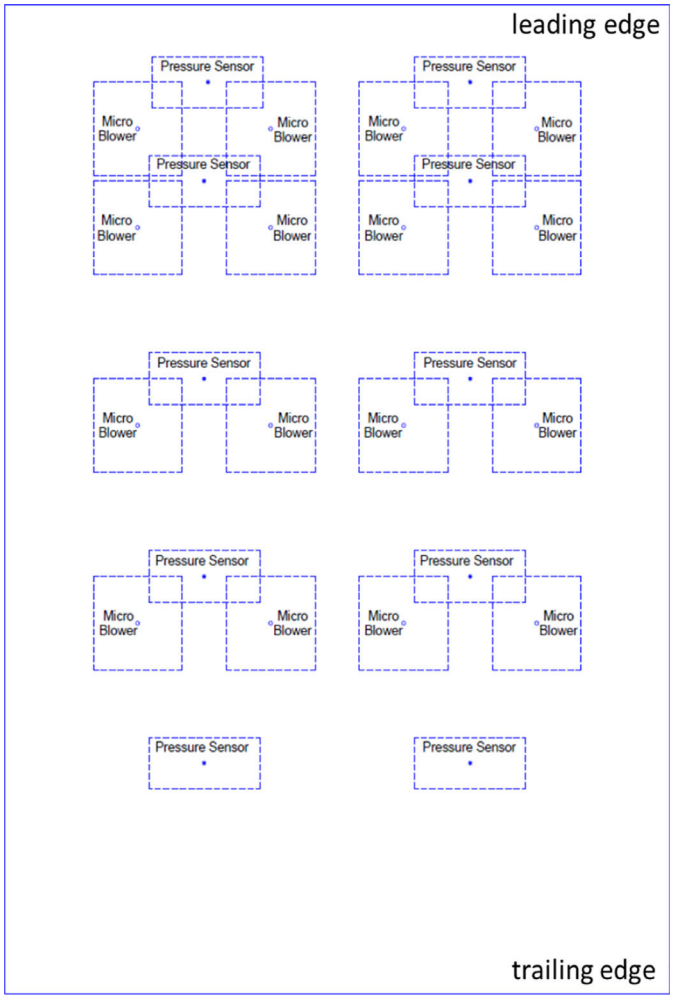

Fig. 13. Layout of actuators and sensors in the active integrated cell.

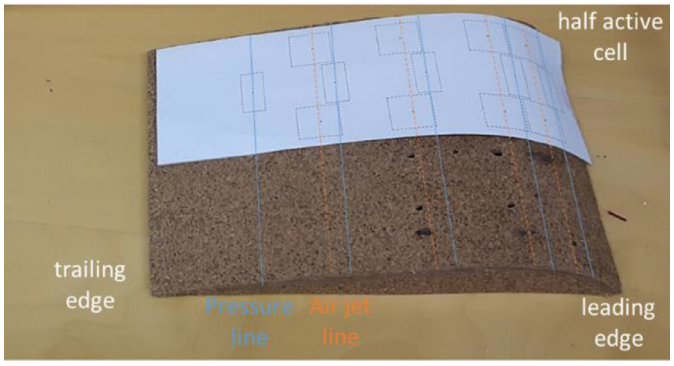

Fig. 14. Active integrated sensor/actuator cell with different pressure and air jet lines along the airfoil.

5.3. Sensors

The selected pressure sensor for the final AFC prototype is Bosch BMP280 [25]. The sensor (individual SMA case) and the driver circuit are shown in Fig. 17. This sensor has an operational range that is more adequate to track turbulence conditions for the envisioned testing conditions of the prototype. In the final wind tunnel prototype, the pressure sensors are also used to evaluate the performance of the active flow control system.

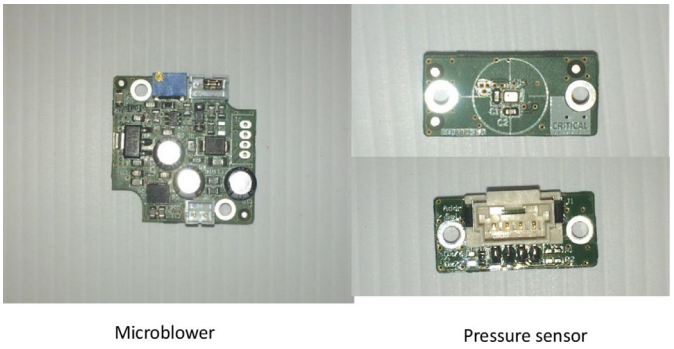

Fig. 15. Interface electronics.

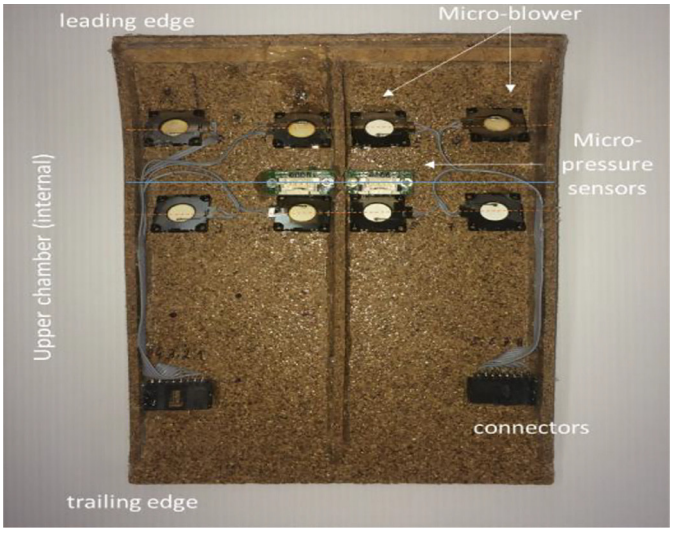

Fig. 16. Mock-up of an instrument upper chamber section.

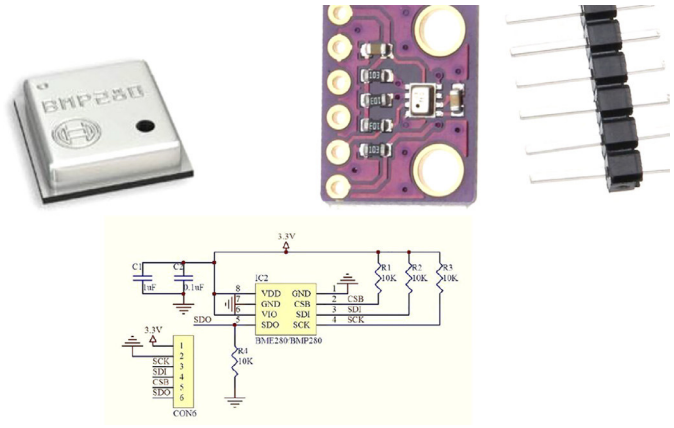

Fig. 17. Bosch BMP pressure sensor and driver circuit [25].

5.4. Actuators

A commercially available micro pump actuator has been selected to be used in the prototype: Piezoelectric Microblower muRata MZB1001T02 [26]. This micro pump mimics with good accuracy the performance of a synthetic actuator. In fact, it can be considered a non-zero mas flux actuator by injecting flow into the main airflow stream above the wing. The envisioned actuators are displayed in Fig. 18.

Fig. 18. Microblowers muRata MZB1001T02 [26].

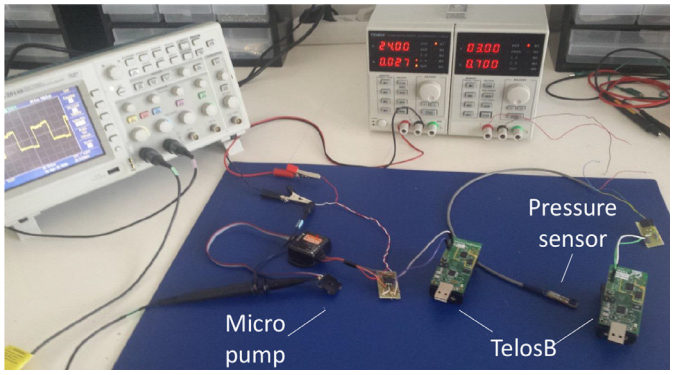

Fig. 19. Integrated actuator and pressure sensor into TelosB node for active flow control.

5.5. Integration with wireless node

The control lines of the Telos-B node [27] have been used to enable the control of the line of actuators. Different actuation policies can be enabled via the wireless connection to the internal aeronautics network, where policies for the whole aircraft can be coordinated. The integration is shown in Figs. 19 and 20. The telos-B node implements ZigBee protocol over IEEE 802.15.4 MAC-PHY technology. This technology is also used in the system level simulation and scalability analysis results displayed in subsequent sections.

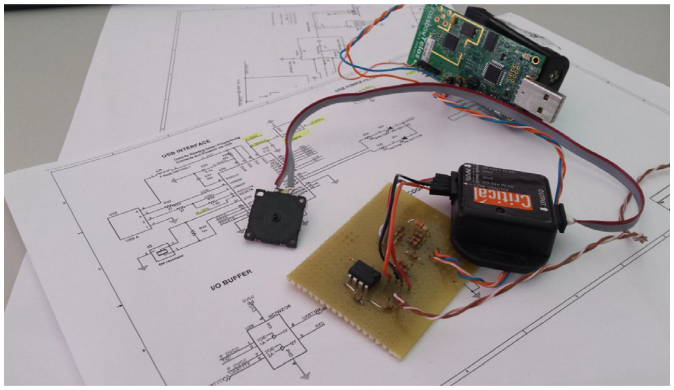

Fig. 20. Integrated actuator and pressure sensor into TelosB node for active flow control.

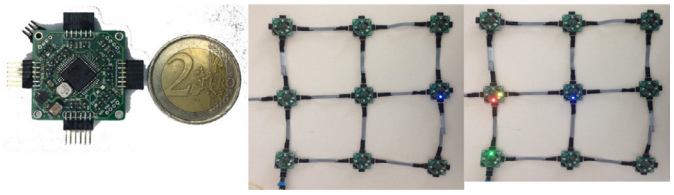

Fig. 21. Microcontroller (left top) and typical testing deployment for a network of connected microcontrollers (right top) for the XDense system.

5.6. Real-time intra-patch network

The prototype has also the option to implement a real time wired network for intra-patch communication with a technology called XDense [28]. In this technology, each node inside the patch contains a microcontroller. Each microcontroller is able to manage several sensors and actuators simultaneously, while communicating with its neighbours using different protocols that have been analysed with the purpose of achieving real time capabilities in grid deployments. Fig. 21 shows the microcontroller board of the XDense technology with integrated pressure and light sensors. Fig. 22 shows a typical deployment in grid configuration to enable the tracking of a free air stream jet. The network of processors implements a boundary detection algorithm that allows the system to track the formation of turbulent flow in real time fashion.

5.7. Load sensor system

One of the main expected outcomes of the AFC system is the reduction of drag friction and consequently the improvement of lift-off forces experience by the wing section. A load sensor has been implemented that is able to detect variations of lift off force experienced by the wing section and consequently the effects of the AFC system. The selected load sensor is RB-Phi-118 from Phidget Bridge [29]. The load sensor is displayed below in Fig. 23 and the driver circuit in Fig. 24.

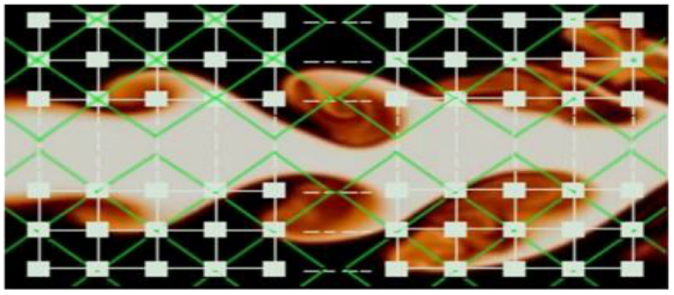

Fig. 22. Deployment of the XDense grid over the simulation of a free air strem jet.

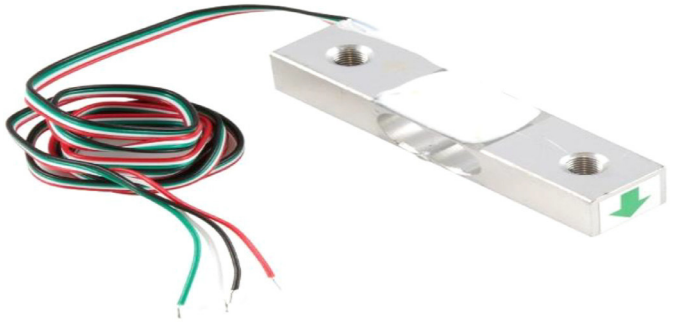

Fig. 23. Micro load sensor RB-Phi-118 from Phidget Bridge [29].

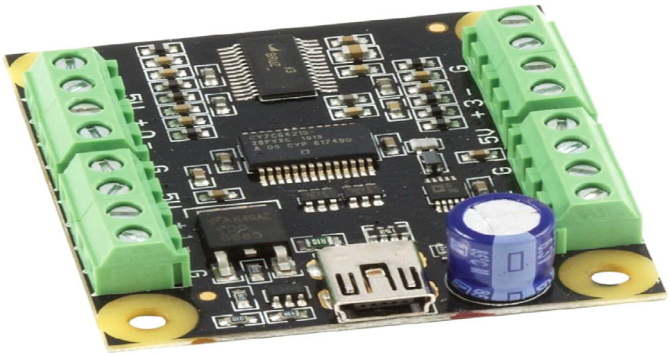

Fig. 24. Load sensor driver system.

Fig. 25. Wind tunnel with open design according to the guidelines in [31].

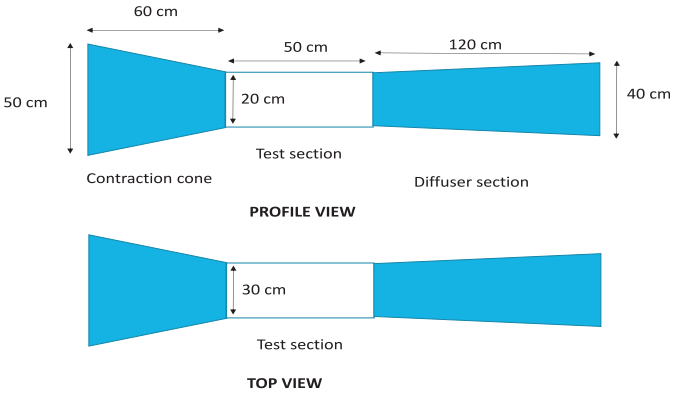

Fig. 26. Wind tunnel schematics.

5.8. Wind tunnel description

The wind tunnel aims to generate appropriate conditions for testing of active flow control at higher wind speeds. The dimensions of this wind tunnel match the directions provided in [31]. Different fans have been used to reproduces different values of wind speed (e.g. [32]). The test section made of pyro glass has dimensions of 30 × 20 × 50 cm. The contraction zone has dimensions of 60 × 60 cm and 30 × 20 cm in both ends with 60 cm long. The section of the fan has dimensions of 45 × 45 cm and 30 × 20 cm in both ends with a length of 120 cm.

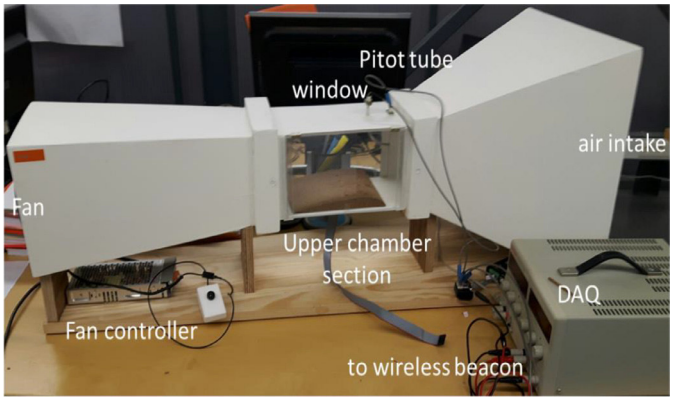

Fig. 27. Experimental small wind tunnel.

The wind tunnel is shown in Fig. 25 and the schematics with dimensions of the different sections of the tunnel in Fig. 26. The main achievement this wind tunnel is the control of wind speed using a variable speed motor driver, and the measurement of the wind speed. This allows us to test under controlled conditions specific patterns of patch design. This contributes to a better understanding of the complex trade-offs between the speed of actuation, the sensor feedback and the design of actuation policies. Fig. 27 shows the small wind tunnel built with the mock-up of the upper chamber inside, and the independent connectors to the wireless beacons.

The wind tunnel has been enabled with a controller software that allows the user to collect the measurements about speed inside the test section, displaying the readings of the pressure sensors on the surface of the wing section, and the different communication commands to control the electronics of the tunnel.

6. CFD simulation results

6.1. Objective

When an airfoil is subject to an air flow on its surface, a force vector is generated on its surface, constituted by two components: *lift* and *drag forces*. The study in this section analyses the influence on these forces when certain air jets are applied on the surface of an airfoil using external pumps with different air speeds. Because this is a complex problem, a computational model is developed to preform different simulations in different conditions using CFD to give some sensitivity to the physics of the problem and identify the variables responsible to fine tune the lift and drag forces on an air foil.

6.2. Scope

This study is to give support on the development of an algorithm to increase the efficiency of an air foil in different air speed conditions. A commercial CFD software tool ABAQUS has been used to obtain the results in this section.

6.3. Description

This section presents the preparatory computational fluid dynamic analyses of a half NACA 0024 airfoil embedded in a wind tunnel subjected to different simulations with the intention to manipulate the drag coefficient (CD) by the means of auxiliary “air micro-blowers” on the upper chamber surface of the airfoil. The following five trials that are presented intend to demonstrate the changeability of CD and CL output results obtained:

1. By different “air injection” velocities over four distinct rows of “air micro-blowers”;

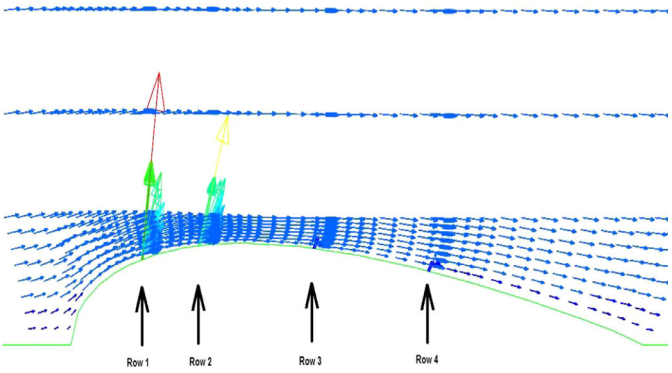

Fig. 28. Visualization of the "air micro-blowers" line-up relative to the airfoil cord.

Table 2
Designation wind tunnel velocities [m/s].

Designation	Wind tunnel velocities [m/s]
S05	5
S06	6
S07	7
S08	8
S09	9
S1	10
S2	20
S3	30
S4	40

Table 3
Analysis One, main definitions.

Designation	Alignment	V injectors	Ang.	V1	V2
	Row 1	41.4	67.5	15.8	38.2
	Row 2	41.4	67.5	15.8	38.2
S05 - T-48P	Row 3	2.5	67.5	1.0	2.3
	Row 4	2.5	67.5	1.0	2.3
S05 - T	–	–	–	–	–

Table 4
Analysis Four, main definitions.

Trials	Alignment	V of air injectors [m/s]	Ang. [°]	V1 [m/s]	V2 [m/s]
S05 - T-24P	Row 1	41.4	67.5	15.8	38.2
	Row 2	41.4	67.5	15.8	38.2
	Row 3	2.5	67.5	1.0	2.3
	Row 4	2.5	67.5	1.0	2.3
S05 - T	–	–	–	–	–

2. By the number of "air micro-blowers" on each of the four rows;
3. By the wind tunnel inlet velocity.

Specifically in all the trials presented, the first two rows of "air micro-blowers" have higher velocities and the following two rows have lower velocities as detailed in Fig. 28.

Table 2 describes the main wind tunnel inlet velocities submitted to CFD simulations. The rest of the tables provide the simulation conditions for five different types of analysis with different number of actuators and different policies of different rows of actuators across the surface of the wing section (Tables 3–8).

6.4. CFD results

The presented simulation results for all five analyses are presented in the tables of results. The results show the different gains in the presented indicators for the different configurations and airflow speeds. These results confirm that the approach with microblowers as actuators are capable of overcoming the different metrics related to skin friction drag. The parameters analysed are given below.

Table 5
Analysis Two, main definitions.

Trials	Alignment	V injectors	Ang.	V1	V2
	Row 1	41.4	67.5	15.8	38.2
	Row 2	41.4	67.5	15.8	38.2
S06 - T-48P	Row 3	2.5	67.5	1.0	2.3
	Row 4	2.5	67.5	1.0	2.3
S06 - T	–	–	–	–	–
	Row 1	41.4	67.5	15.8	38.2
	Row 2	41.4	67.5	15.8	38.2
S07 - T-48P	Row 3	2.5	67.5	1.0	2.3
	Row 4	2.5	67.5	1.0	2.3
S07 - T	–	–	–	–	–
	Row 1	41.4	67.5	15.8	38.2
	Row 2	41.4	67.5	15.8	38.2
S08 - T-48P	Row 3	2.5	67.5	1.0	2.3
	Row 4	2.5	67.5	1.0	2.3
S08 - T	–	–	–	–	–
	Row 1	41.4	67.5	15.8	38.2
	Row 2	41.4	67.5	15.8	38.2
S09 - T-48P	Row 3	2.5	67.5	1.0	2.3
	Row 4	2.5	67.5	1.0	2.3
S09 - T	–	–	–	–	–

Table 6
Analysis three, main definitions.

Trials	Alignment	V injectors	Ang.	V1	V2
	Row 1	41.4	67.5	15.8	38.2
	Row 2	41.4	67.5	15.8	38.2
S05 - T-48P	Row 3	2.5	67.5	1.0	2.3
	Row 4	2.5	67.5	1.0	2.3
S05-T	–	–	–	–	–
	Row 1	82.8	67.5	31.7	76.5
	Row 2	82.8	67.5	31.7	76.5
S1 - T-48P	Row 3	5	67.5	1.9	4.6
	Row 4	5	67.5	1.9	4.6
S01 - T	–	–	–	–	–
	Row 1	165.6	67.5	63.4	153
	Row 2	165.6	67.5	63.4	153
S2 - T-48P	Row 3	10	67.5	3.8	9.2
	Row 4	10	67.5	3.8	9.2
S2 - T	–	–	–	–	–
	Row 1	248.4	67.5	95.1	229.5
	Row 2	248.4	67.5	95.1	229.5
S3 - T-48P	Row 3	67.5	67.5	5.7	13.9
	Row 4	15	67.5	5.7	13.9
S3 - T	–	–	–	–	–
	Row 1	331.5	67.5	126.9	306.3
	Row 2	331.5	67.5	126.9	306.3
S4 - T-48P	Row 3	20	67.5	7.7	18.5
	Row 4	20	67.5	7.7	18.5
S4 - T	–	–	–	–	–

Table 7
Analysis Five, main definitions.

Trials	Alignment	V injectors	Ang.	V1	V2
	Row 1	41.4	67.5	15.8	38.2
	Row 2	41.4	67.5	15.8	38.2
S05 - T-16P	Row 3	67.5	15.8	1.0	38.2
	Row 4	41.4	67.5	1.0	38.2
S05 - T	–	–	–	–	–

Table 8
Results CFD.

Trials	ν	ξ	θ	η
Analysis One				
S05-T	0.0199	0.0167	0.3645	0.3053
S05-T-48P	0.0162	0.0136	0.3875	0.3246
Analysis Two				
S06-T	0.0190	0.0229	0.3671	0.4429
S06-T-48P	0.0167	0.0201	0.3830	0.4621
S07-T	0.0183	0.03	0.3692	0.6062
S07-T-48P	0.0168	0.0276	0.3808	0.6252
S08-T	0.0177	0.0380	0.3708	0.7953
S08-T-48P	0.0167	0.0359	0.3796	0.8142
S09-T	0.0173	0.0469	0.3722	1.0103
S09-T-48P	0.0166	0.0451	0.3791	1.029
Analysis Three				
S1-T	0.0169	0.0567	0.3734	1.2513
S1-T-48P	0.0135	0.0451	0.3969	1.3301
S2-T	0.0150	0.2017	0.3801	5.0944
S2-T-48P	0.0116	0.1560	0.4039	5.4135
S3-T	0.0143	0.4307	0.3832	11.5584
S3-T-48P	0.0109	0.3278	0.4072	12.2811
S4-T	0.0138	0.7409	0.3853	20.6562
S4-T-48P	0.01	0.5377	0.4093	21.9462
Analysis Four				
S05-T	0.0199	0.0167	0.3645	0.3053
S05-T-24P	0.0179	0.0150	0.3751	0.3142
Analysis Five				
S05-T	0.0199	0.0167	0.3645	0.3053
S05-T-16P	0.0189	0.0158	0.3707	0.3105

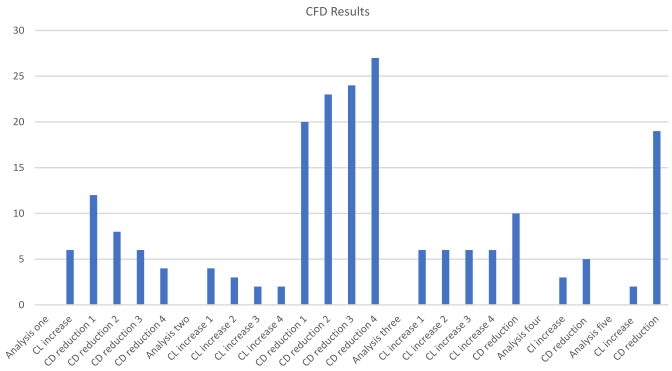

Fig. 29. Summary of CFD results.

1. Drag Coefficient - CD: ν
2. Drag Force: ξ
3. Lift Coefficient - CL: θ
4. Lift Force η

For analysis one, the simulation results show a CL Total increase of 6%, a CD Total reduction of 12%, 8%, 6% and 4%. For analysis two, the simulation results show a CL Total increase of 4%, 3%, 2% and 2%, and a CD Total reduction of 20%, 23%, 24% and 27%. For analysis three, the simulation results show a CL Total increase of 6%, 6%, 6% and 6% ,and a CD Total reduction of 10%. For analysis four, the results show a CL Total increase of 3% and a CD Total reduction of 5%. For analysis five, the simulation results show a CL Total increase of 2% and a CD Total reduction of 19%. These results show the potential gains using microblowers over a wing section inside an experimental wind tunnel, as shown in next subsection. A summary of these results is displayed in Fig. 29.

7. Results

This subsection provides an update on the simulation work performed for the AFC system. The simulation parameters of this tool can be found in Fig. 10. The results of CFD simulation have to be imported off-line into the wireless simulator using a statistical modelling approach similar to the tools used in wireless channel modelling. Fig. 30 shows a snapshot of the results of boundary layer formation using an angle of attack of 24°. The figure shows in circles the instances (random) of the point where turbulent flow starts to form (separation layer). The turbulent model used the statistics of the CFD using an infinite series expansion of chi-square distributions. Fig. 30 shows the profile of a wing, while Fig. 31 presents the view from above the wing,

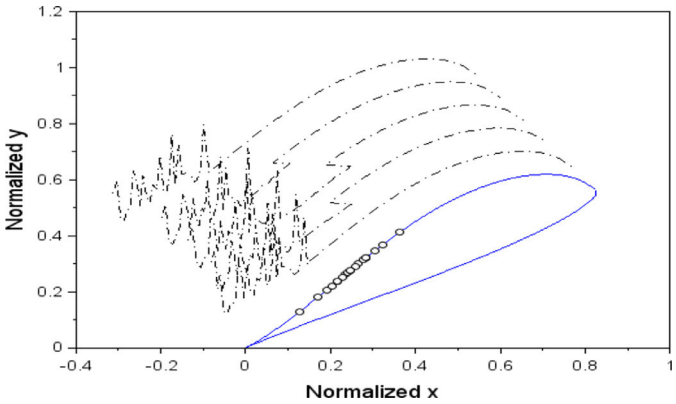

Fig. 30. Turbulent boundary layer formation simulation results with an angle of attack (AoA) of 24° (Wing profile).

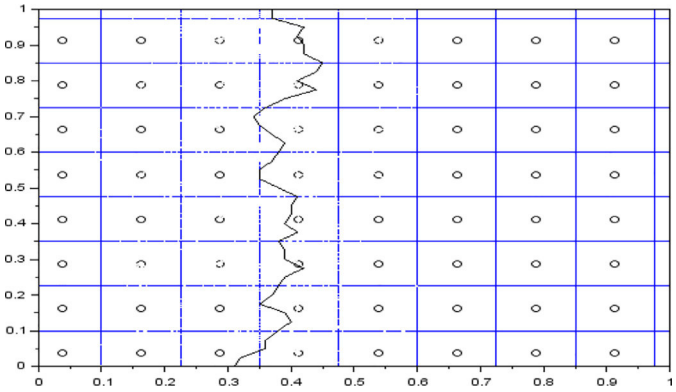

Fig. 31. Turbulent boundary layer formations (simulation results) with an angle of attack (AoA) of 24° (Vision from above of the wing).

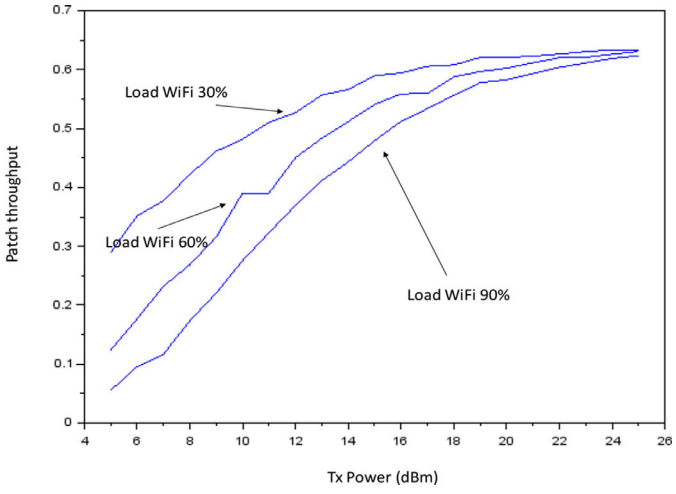

Fig. 32. Throughput versus Tx power for the system level simulation of the active flow control system: Time-slot allocation.

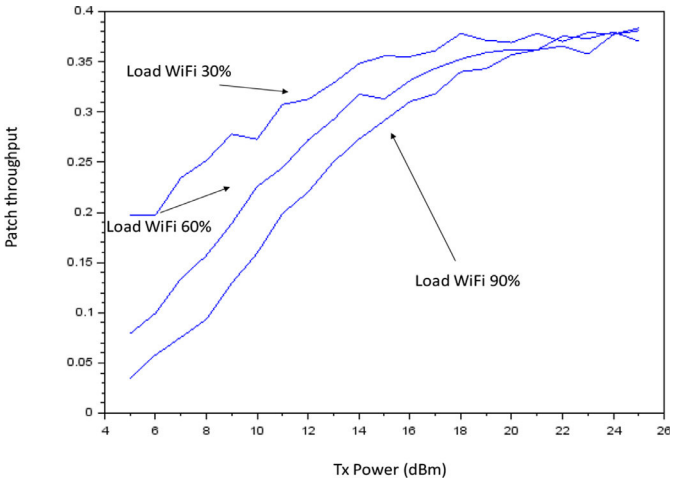

Fig. 33. Throughput versus Tx power for the system level simulation of the active flow control system: Contention-based operation.

Table 9
Simulation parameters.

Parameter	Description
Operational frequency	2.4 GHz
Bandwidth	5 MHz
Thermal noise	5 MHz
Propagation model	ITU WAICS internal and external model
Frame length	15 ms contention free
PHY layer modulation	IEEE 802.15.4
MAC layer	Contention free
Tx power	20 dBm
Interference model	ITU WAICS internal and external model
Power control	No
Simulator mode	Combined snap-shot
Interference model	ITU WAICS internal and external model
LSLI model	Instantaneous SINR mapping over AWGN
Antenna radiation pattern	Omnidirectional
Scheduler	Round robin
CFD interface	Correlated spatial-temporal envelope model
Patch size	Configurable 10–100 cm
No of patches	Configurable 1–50 nodes

using straight lines to denote the boundary layer formed randomly. These lines constitute the main element that will be tracked to try to counteract the effects of turbulence via actuators.

The results of system level patch throughput in Figs. 32 and 33 have been obtained for a network of patches operating with ZigBee protocol, under the assumption of interference from a co-channel Wifi network operating inside the aircraft. ITU propagation model for WAICs has been implemented. All the simulation parameters can be found in Table 9. The results show the overall performance of throughput for all the patches in the aircraft. The values of throughput can also be used in conjunction with the CFD results of the previous section to obtain an overall skin friction reduction percentage for the whole aircraft of about 10% depending on the traffic load. More importantly we have demonstrated how to perform a system level simulation of an active flow control system and how to introduce the results of the CFD simulation for the fluid performance in the presence of sensors and actuators. The simulation results also show that the use of wireless can provide some gains, particularly for medium term and spatial components of the turbulent flow in the order of 10 cm and 100 Hz. This value provides a good trade-off between the capacity of the intra-patch and inter patch communication technology. It is possible to use wireless and wireline transmission technologies with more capacity and therefore address turbulence components of higher order, and thus increase the efficiency of the skin friction reduction and lift off forces. The overall gains of lift

Table 10
Results prototype.

AoA	A. speed (m/s)	Frequency (Hz)	Load gain
0	16	10 KHz	Av. 18 Std. 2.5
10	16	10 KHz	Av. 22 Std. 3.3
20	16	10 KHz	Av. 10 Std. 2.1
30	16	10 KHz	Av. -3 Std. 1.2

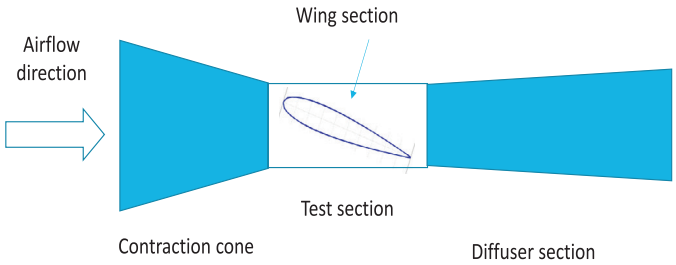

Fig. 34. Set up for prototype testing using different values of angle of attack (AoA).

Fig. 35. Graphical user interface showing the effects of wing surface pressure of the activation of the actuation policies.

off forces can be translated directly into fuel increased efficiency, depending on the aircraft configuration, payload, range, etc. Future work remains in improving the structure of the simulator, the models of interaction between the CFD and the network simulation world, and of course in the prototype development to address higher flow air speeds and higher order turbulence statistical components in space and time.

The results of the prototype measurement are displayed in Table 10 using the setup testing with different angles of attack (AoA) as shown in Fig. 34. The graphical user interface (GUI) of the wind tunnel testbed is displayed in Fig. 35. This GUI shows the value of pressure over the surface of the wings inside the testing chamber. The values of the prototype could not be directly correlated with the results of simulation due to the limitations of the testing bed. However, the gains in lift and pressure obtained in the prototype test confirm the idea of drag reduction over the surface of the wing sections tested.

8. Scalability and sizing study

Let us now address a formal calculation of the size of the network given the analysis of turbulence flow to be managed. The number of sensor nodes per patch is denoted by N_s and the number of actuators by N_a. Our first assumption is regarding the actuation policy. The simplest possible policy is binary policy: on and off. This means that the actuators will be simply switched on when any type of turbulence is detected or switched off if laminar flow is present. Under this assumption, the first rule derived is that the number of sensors is lower or equal than

the number of actuators (binary actuation policy decision):

$$N_s \geq N_a$$

Note the relevance of the actuation policy. Different actuation policies are possible. For example, amplitude and frequency of the piezoelectric material in the actuator can be adjusted according to different measurements of turbulence or according to a model that predicts the need of different levels of actuation inside the turbulent flow area. Under the worst case scenario, the density of sensing and actuation should be as small as 0.1 mm @ 100 kHz (denoted here by Δ_s and f, respectively). On the other hand, in the best case scenario, we are looking at sensing rates of the order of 1 cm @ 1 kHz or even 10 cm @ 100 Hz to track the medium term statistics of the boundary separation layer.

To obtain the number of sensors and actuators per patch, let us now focus on the data transport algorithm inside the patch. There are many possible combinations for algorithms inside the patch. For simplicity, we will consider a bus configuration that will allows us to obtain closed-form expressions for the number of required nodes in a patch. For other transport algorithms and network configurations such as Manhattan grid and multi-hop data transport, in general simulation in NS-3 will be required. Let us now consider Ethernet as the baseband transport technology inside a patch with $R_b = 100$ Gbps capacity. In the worst case scenario, the sensing data rate per sensor, considering 8-bit representation, approximately of 800 kbps plus overhead resulting in a rough estimate of $R_s = 1$ Mbps. This means each patch can potentially host up 100 k sensors, which in a rectangular patch means approximately 300 sensors per side. This is obviously optimistic, mainly because of potential collisions or transmission errors in the physical and MAC layers. Using a 50% margin ($\mu = 0.5$), one patch could host 50,000 sensors using 100 Gbps Ethernet, or 50 for 100 Mbps Ethernet. In the Ethernet version implemented by AFDX of the aeronautical internal communication network, 100 Mbps is the maximum data rate. The above calculation can be expressed mathematically as follows:

$$N_s = (\mu R_b)/R_s$$

where μ is the compression rate or design margin, R is the rate of the bus technology, and $R_s = 10f$ is the rate per sensor. To conclude, we can say that in the worst case scenario, approximately 50 sensor nodes can be host ed per patch using AFDX Ethernet in shared bus configuration. Other data transmission configurations that can improve this figure at the expense of further processing per sensor node or delay in processing multi-hop configurations. It is also possible to enable local processing per sensor node and only transport compressed information inside the patch. The physical size of the patch can be obtained as follows:

$$l = \Delta_s \sqrt{N_s}$$

Note that the sizes of the patch in the worst case scenario boils down to only 2.2 cm when using 100 Gbps Ethernet or 0.07 cm with 100 Mbps Ethernet. These sizes of a patch are too small. This means that inside the patch only a limited number of sensors can be wired together when dealing with the micro scale turbulent component. In the best case scenario, the estimate data rate number goes up to 10 kbps or 1 kbps. Using 100 Mbps Ethernet and following the lines of the previous calculation, the estimated number of sensors per patch increases to 5000 and 50,000, respectively. However, the size of the patch will be mainly limited by the wireless technology used for patch to sink node communication. Assuming IEEE 802.15.4 technology for a patch with a capacity of 250 kbps, the maximum number of nodes per patch could be obtained as 12 or 125 when dealing with the small-scale statistics of turbulence (our best case scenario). However, this calculation assumes that there is only one patch in the network. Considering time-slot operation of IEEE802.15.4, $N_p = 7$ patches can transmit simultaneously sharing the overall data rate. Therefore, the number of nodes per patch can go down to only 2 or 13, respectively. On the other hand, if Wi-Fi technology is employed with 600 Mbps, this number can go up to 60 or 600 assuming heavy losses by collisions ($\mu/N_p = 0.01$,). This can be

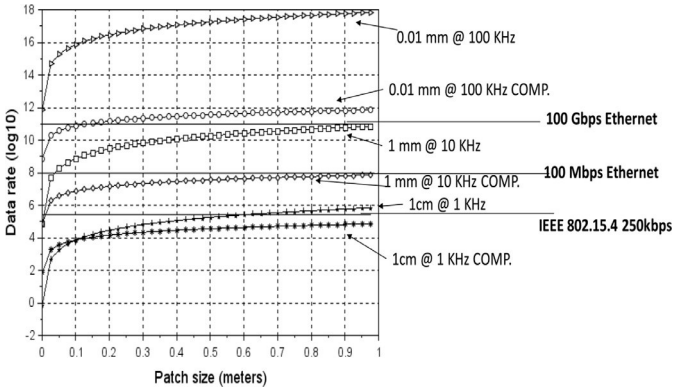

Fig. 36. Scalability analysis of the proposed Wireless AFC system.

expressed as follows:

$$N_s = (\mu R_c)/(N_p r_s)$$

where N_p is the number of patches per radio channel and R_c is the data rate per radio channel. Regarding the size of the patch with IEEE 802.15.4 the size can be as small as 1.3 cm or 42 cm per side. This latter result corresponds to the case with 10 cm @ 100 Hz sensing rates. Also note that it is possible to use more sensors for inside patch processing and then compress the information (subsample) for communication with the wireless network. This offers several possibilities for realization of the patch and the deployment of the aeronautics DEWI Bubble. Fig. 36 shows the results of capacity-scaling considering different wireless and wireline technologies for different values of temporal and spatial sampling and the use of compression with perfect boundary detection assumption (Only the information of the boundary layer curve is relayed by the patch).

9. Conclusions and future work

This paper has presented the design of the AFC system based on a dense wireless sensor and actuator network using the concept of the DEWI Bubble. The paper presented the architecture of the system, the description of the modules and elements that are critical for the operation of tracking turbulent formation across the surface of the fuselage of aircraft. The paper also described a simulator that is being used to design different aspects of the systems including scalability analysis. Simulation results show the interactions between the fluid physical world and the wireless sensor domain. CFD simulation results were used to design the physical prototype of a section of a wing with a set of sensors and actuators. The details of the prototype, the testbed (wind tunnel) and the results of measuring the influence of actuators on the aerodynamic performance of the selected wing profile are here described. There is also an updated results of system level simulation considering a dense wireless sensor and actuators grouped into units called patches. The system level simulation assumes a realistic propagation model inside a commercial aircraft and the effect of interference from a WiFi network that is assumed to operate inside the cabin of the aircraft. The results highlight the importance of the use of the wireless component to provide modularity, flexible implementation, and management capabilities to a dense wireless sensor and actuator network that is used for purposes of active flow control. The paper also shows the potential to use modern wireless technologies in the aeronautics industry to enable high level applications, achieving connectivity with internal networks of commercial aircraft and with ground control. This is expected to enable smart avionics applications. Future work lies in the potential security and safety threats that can affect the performance for the active flow control systems or any other structure health monitoring system in commercial aircraft. This security, safety and trustiness analysis will be conducted in the European ECSEL project SCOTT

(secure connected trustable things) that aims to continue and improve the results of the parent project DEWI.

Acknowledgement

The research from DEWI project (www.dewi-project.eu) has received funding from the ARTEMIS Joint Undertaking under grant agreement No. 621353. SCOTT (www.scottproject.eu) has received funding from the Electronic Component Systems for European Leadership Joint Undertaking under grant agreement No 737422. This Joint Undertaking receives support from the European Unions Horizon 2020 research and innovation programme and Austria, Spain, Finland, Ireland, Sweden, Germany, Poland, Portugal, Netherlands, Belgium, Norway. Funded also by FCT/MEC (Fundacão para a Ciência e a Tecnologia), ERDF (European Regional Development Fund) under PT2020, and by CISTER Research Unit (CEC/04234)

Supplementary material

Supplementary material associated with this article can be found, in the online version, at doi:10.1016/j.micpro.2018.05.012

References

[1] C. Sky, Available at http://www.cleansky.eu/.
[2] S.G. Anders, W.L. Sellers, A.E. Washburn, “Active flow control activities at NASA langley,”, 2nd AIAA Flow Control Conference,June 28 - July 1, (2004).
[3] T. Washburn, “Airframe drag/weight reduction technologies,”, Green Aviation Summit - Fuel Burn Reduction, NASA Ames Research Centre (2010). September
[4] A.M. Carry, D.M. Bushnell, J.W. Hefner, “Slot injection for skin friction drag reduction,”, AGAR Rept. 654, (1977).
[5] J. Reneaux, “Overview of drag reduction technologies for civil transport aircraft,”, European Congress on Computational Methods in Applied Sciences and Engineering (ECCOMAS), (2004).
[6] I. Martnez, Aircraft propulsion, Available Online at http://webserver.dmt.upm.es/?isidoro/bk3/c17/Aircraft%20propulsion.pdf.
[7] L. Prandtl, Uber flussigkeitsbewegung bei sehr kleiner reibung, in: Third International Congress of Mathematicians, Heidelberg, pp. 484–491.
[8] M. Watson, A.J. Jaworski, N.J. Wood, “Application of synthetic jet actuators for the modification of the characteristics of separated shear layers on slender wings,”, Aeronaut. J. 111 (August (1122)) (2007) 519–529.
[9] B.G. Allan, N. Langley, “progress towards fuselage drag reduction via active flow control : A combined CFD and experimental effort,”, 36th European Rotorcraft Forum; 7–9 Sep. Paris; France, (2010).
[10] Joslin, Miller, “fundamentals and applications of modern flow control,”, American Institute of Aeronautics and Astronautics.
[11] U. Buder, L. Henning, A. Neumann, “aeroMEMS wall hot-wire sensor arrays on polyimide with through foil vias and bottom side electrical contacts,”, International Solid-State Sensors, Actuators and Microsystems Conference, Lyon, (2007), pp. 2333–2336.
[12] AEROMEMSII, “advanced aerodynamic flow control using MEMS,”, [Online]. Available: http://cordis.europa.eu/project/rcn/61956_en.html.
[13] U. Buder, R. Petz, M. Kittel, W. Nitsche, E. Obermeier, “aeroMEMS polyimide based wall double hot-wire sensors for flow separation detection,”, Sens. Actuat. A 142 (March (1)) (2008) 130–137.
[14] M. Schober, E. Obermeier, S. Pirskawetz, H.H. Fernholz, “a MEMS skin-friction sensor for time resolved measurements in separated flows,”, Exp. Fluids, 36 (April (4)) (2004) 593–599.
[15] J.M. Engel, S. Member, J. Chen, C. Liu, S. Member, “Polyurethane rubber all-polymer artificial hair cell sensor,”, J. Microelectromech. Syst. 15 (4) (2006) 729–736.
[16] N. Chen, C. Tucker, J.M. Engel, Y. Yang, S. Pandya, C. Liu, “Design and characterization of artificial haircell sensor for flow sensing with ultrahigh velocity and angular sensitivity,”, J. Microelectromech. Syst. 16 (5) (2007) 999–1014.
[17] L.N. Cattafesta, M. Sheplak, “Actuators for active flow control,”, Annu. Rev. Fluid Mech. 43 (1) (2011) 247–272. Jan.
[18] A. Glezer, M. Amitay, “Synthetic jets,”, Annu. Rev. Fluid Mech. (2002).
[19] C. Warsop, Advanced flow control using MEMS results and lessons learned, 5th Community Aeronautical Days 2006, Vienna, Austria, (2006).
[20] K. Kingery, Electromagnetic water cloak eliminates drag and wake, 2017, December 11, Duke University. Read more at: https://phys.org/news/2017-12-electromagnetic-cloak.html.
[21] J.U. DEWI, Grant agreement annex 1 - description of work, 2015, -03-04.
[22] F.J. Diez, W.J.A. Dahm, “Electrokinetic microactuator arrays and system architecture for active sublayer control of turbulent boundary layers,”, AIAA J. 41 (10) (2003) 1906–1915.
[23] H. Suzuki, N. Kasagi, Y. Suzuki, “Active control of an axisymmetric jet with distributed electromagnetic flap actuators,”, Exp. Fluids, 36 (March (3)) (2004) 498–509.
[24] K.S. Choi, T. Jukes, R. Whalley, “Turbulent boundary-layer control with plasma actuators,”, Philos. Trans. R. Soc. A 369 (1940) (2011) 1443–1458.
[25] B. BMP280, 2016, Data sheet. https://cdn-shop.adafruit.com/datasheets/BST-BMP280-DS001-11.pdf. Last accessed December.
[26] M. microblower, 2016, MZB1001T02. Data sheet: http://www.mouser.com/ds/2/281/Murata_MZB1001T02_datasheet-493611.pdf. Last accessed December.
[27] B. Telos, 2016, MEMSIC wireless node. http://www.memsic.com/userfiles/files/Datasheets/WSN/telosb_datasheet.pdf. Last accessed December.
[28] J. Loureiro, R. Raghu, E. Tovar, “Experiments with XDense: A Dense Grid Sensor Network for Distributed Feature Extraction,”, “Communications in Computer and Information Science book series (CCIS, volume 702),”, (2017), pp. 1–22. Chapter in Springer International. 12, July.
[29] L. sensor, 2016, RB-Phi-118 phidgets. http://www.robotshop.com/ca/en/micro-load-cell-5-kg.html. Last accessed December.
[30] J. Moran, An introduction to theoretical and computational aerodynamics, 1984, Dover editorial.
[31] R.p. w. tunnel, 2016, http://www.instructables.com/id/DIY-Subsonic-Wind-Tunnel-LiftDrag-Testing-for-RLoo/. Last accessed December.
[32] E.-p. W2S130-AA03-01, 2016, Technical features https://www.soselectronic.hu/productdata/52/01/7/52017/W2S130AA0301-ENG.pdf. Last accessed December 2016 Last accessed December.
[33] J.Cramer, "Update on WRC-12 issues impacting Wireless Avionics Intracommunications", ITU-R Working Party 5B and Future regulatory Considerations.
[34] ITU-R M.2197-0 (2010). Technical characteristics and operational objectives for Wireless avionics intra-communications (WAIC).

Ramiro Samano Robles obtained his degree in Telecommunications engineering from the national university of Mexico in 2001. He obtained the PhD in signal processing for wireless communications from the University of Leeds in 2007, and MSc in Telecommunications and Information Systems from the University of Essex in 2003. He held a postdoctoral position at the Institute of Telecommunications in Aveiro, Portugal, where he was involved in the management and scientific contribution of several FCT and FP7 European research projects related to distributed MIMO, RFID, Internet of things (IOT), radio-over-fibre distributed antenna systems, cooperative systems, and cognitive radio. He currently hols a research associate position at the Research center on real time and embedded computing systems in Porto, Portugal.

Julio Viana is CTO. PhD in Polymer Sci. and Eng, with expertise on mechanically active polymers and advance polymer processing for Aeronautics and automotive. He coordinated several scientific and industrial projects.

Nelson Ferreira is expert in Electronic and Instrumentation, with a MEng and MSc in Electronic Eng. (Robotics and Automation). Senior Engineer at CMT and EI Laboratory responsible. Skills on telemetry and data acquisition, automation, project management, system integration, design of electronic hardware and software.

João Loureiro holds a degree in Mechatronic Engineer since 2009 from Pontifcia Universidade Catlica de Minas Gerais, Brazil. He has worked in research and development of embedded systems, both inside industry and university. His research interests are in Real Time Embedded Systems, Cyber-Physical Systems and Sensor Networks. Currently his research is includes the development of a network architecture for extreme dense sensing for active flow control. Joo Loureiro is a PhD candidate in Electrical and Computer Engineering in FEUP and researcher at the CISTER Research Unit.

João Cintra - Project Manager With a more than 15-years IT consultant background, he is a project manager since 2005 in a very broad number of domains. In the last projects he is being focused on aeronautics projects with incidence in IMA technologies.

Eduardo Tovar was born in 1967 and has received the Licentiate, MSc and PhD degrees in electrical and computer engineering from the University of Porto, Porto, Portugal, in 1990, 1995 and 1999, respectively. Currently he his Professor in the Computer Engineering Department at the School of Engineering (ISEP) of Polytechnic Institute of Porto (IPP), where he is also engaged in research on real-time distributed systems, wireless sensor networks, multiprocessor systems, cyber-physical systems and industrial communication systems. He heads the CISTER Research Unit, an internationally renowned research centre focusing on RTD in real-time and embedded computing systems. He is deeply engaged in research on real-time distributed systems, multiprocessor systems, cyber-physical systems and industrial communication systems. He is currently the Vice-chair of ACM SIGBED (ACM Special Interest Group on Embedded Computing Systems) and was for 5 years, until December 2015, member of the Executive Committee of the IEEE Technical Committee on Real-Time Systems (TC-RTS). Since 1991 he authored or co-authored more than 150 scientific and technical papers in the area of real-time and embedded computing systems, with emphasis on multiprocessor systems and distributed embedded systems. Eduardo Tovar has been consistently participating in top-rated scientific events as member of the Program Committee, as Program Chair or as General Chair. Notably he has been program chair/co-chair for ECRTS 2005, IEEE RTCSA 2010, IEEE RTAS 2013 or IEEE RTCSA 2016, all in the area of real-time computing systems. He has also been program chair/co-chair of other key scientific events in the area of architectures for computing systems and cyber-physical systems as is the case of ARCS 2014 or the ACM/IEEE ICCPS 2016 or in the area of industrial communications (IEEE WFCS 2014).